



Optimizing observations of drizzle onset with millimeter-wavelength radars

Claudia Acquistapace¹, Stefan Kneifel¹, Ulrich Löhnert¹, Pavlos Kollias^{2,1}, Maximilian Maahn^{3,4}, and Matthias Bauer-Pfundstein⁵

¹University of Cologne, Pohligstr. 3, 50969 Köln (DE)

²Stony Brook University, Stony Brook, NY 11794-5000 (USA)

³Cooperative Institute for Research in Environmental Sciences, University of Colorado, 216 UCB, Boulder, CO 80309, USA

⁴Earth System Research Laboratory, National Oceanographic and Atmospheric Administration, 325 Broadway, Boulder, CO 80305, USA

⁵METEK Meteorologische Messtechnik GmbH, Fritz-Straßmann-Straße 4, 25337 Elmshorn (DE)

Correspondence to: Claudia Acquistapace (cacquist@meteo.uni-koeln.de)

Abstract. Cloud Doppler radars are increasingly used to study cloud and precipitation microphysical processes. Typical bulk cloud properties such as liquid or ice content are usually derived using the first three standard moments of the radar Doppler spectrum. Recent studies demonstrated the value of higher moments for the reduction of retrieval uncertainties and for providing additional insights into microphysical processes. Large effort has been undertaken e.g. within the Atmospheric Radiation Measurement (ARM) program to ensure high quality of radar Doppler spectra. However, a systematic approach concerning the accuracy of higher moments estimates and their sensitivity to basic radar system settings such as spectral resolution, integration time, and beam width is still missing.

In this study we present an approach how to optimize radar settings for radar Doppler spectra moments in the specific context of drizzle detection. The process of drizzle development has shown to be particularly sensitive to higher radar moments such as skewness. We collected radar raw data (IQ time series) from consecutive zenith pointing observations for two liquid cloud cases observed at the cloud observatory JOYCE in Germany. The IQ data allowed us to process Doppler spectra and derive their moments using different spectral resolutions and integration times during identical time intervals. This enabled us to study the sensitivity of the spatio-temporal structure of the derived moments to the different radar settings. The observed signatures were further investigated using a radar Doppler forward model which allowed us to compare observed and simulated sensitivities and also to study the impact of additional hardware-dependent parameters such as antenna beam width.

For the observed cloud with drizzle onset we found that longer integration times mainly modify spectral width (S_w) and skewness (S_k) leaving other moments mostly unaffected. An integration time of 2 s seems to be an optimal compromise: both observations and simulations revealed that a 10 s integration time – as it is widely used for European cloud radars – leads to a significantly turbulence induced increase of S_w and reduction of S_k compared to 2 s integration time. This can lead to significantly different microphysical interpretations with respect to drizzle water content and effective radius. A change from 2 s to even shorter integration times (0.4 s) has much smaller effects on S_w and S_k . We also find that spectral resolution has a small impact on the moment estimations, and thus on the microphysical interpretation of the drizzle signal. Even the coarsest spectral



resolution studied of 0.08 ms^{-1} seems to be appropriate for calculation moments of drizzling clouds. Moreover, simulations provided additional insight into the microphysical interpretation of the skewness signatures observed: in low (high) turbulence condition, only drizzle larger than $20 \mu\text{m}$ ($40 \mu\text{m}$) can generate S_k values above the S_k noise level (in our case 0.4). Higher S_k values are also obtained in simulations when smaller beam widths are adopted.

5 1 Introduction

Millimeter wavelength (cloud) radars are a key component of ground based remote sensing because of their ability to detect and penetrate most cloud types, thus providing vertically-resolved cloud structure. The number of cloud radars around the world and the range of their application in weather and climate research have experienced significant growth in the last 20 years (e.g. Kollias et al., 2007a; Illingworth et al., 2007; Löhnert et al., 2011; Görsdorf et al., 2015; Kollias et al., 2016). The majority of worldwide installed cloud radars are Doppler radars with the ability to record the full Doppler spectrum. The Doppler spectrum provides the distribution of target backscatter as a function of Doppler velocity and when recorded in zenith-mode, it gives information about their vertical motion (Atlas et al., 1973). Commonly, Doppler spectra are not directly used but several moments are derived from them: the first two moments (equivalent radar reflectivity factor Z_e , mean Doppler velocity V_d) are most widely exploited while microphysical studies increasingly make use of higher moments such as spectral width (S_w), skewness (S_k) and kurtosis (e.g. Kollias et al., 2011a; Luke and Kollias, 2013; Maahn et al., 2015; Maahn and Löhnert, 2016).

Considering warm clouds, the formation of drizzle in stratocumulus clouds and the characterization of its signatures in radar Doppler spectra has been of particular interest during the last decades. Gossard (1994), Frisch et al. (1995), and Gossard et al. (1997) developed retrieval techniques exploiting reflectivity, mean Doppler velocity and spectral width to derive drizzle and cloud drop size distributions. Cloud radar observations have also been combined with other remote sensors like microwave radiometers (e.g. Frisch et al., 1995) and lidar (e.g. O'Connor et al., 2005). Kollias et al. (2011a) showed the added value of higher radar moments like skewness and kurtosis for drizzle studies using forward simulations of radar Doppler spectra. They found that particularly the combined signatures of reflectivity and skewness are very sensitive to early drizzle formation. The theoretical findings have been confirmed by a detailed observational study (Kollias et al., 2011b) where the authors also compared the observed vertical evolution of the signatures with drizzle simulations using a 1D bin microphysical model. In a follow-up study, Luke and Kollias (2013) developed a retrieval of drizzle particle size distribution based on the deconvolution of cloud and drizzle peak in regions where drizzle presence was identified by positive skewness.

Kollias et al. (2011a, b); Luke and Kollias (2013) highlighted the importance of high quality (artifact free) radar Doppler spectra collected with high spectral velocity resolution (Kollias et al., 2007b). The current generation of the US Department of Energy Atmospheric Radiation Measurements (ARM) program profiling W and Ka band cloud radars use sampling strategies that enable the detection of microphysical signatures (Kollias et al., 2016). These strategies have been developed based on long-term experience and extensive data analysis for various cloud types. The majority of cloud radars installed across Europe are Ka-band systems of the type MICrowave RAdar (MIRA) manufactured by METEK GmbH (Tab. 1) (Görsdorf et al., 2015). Their number strongly increased during the last ten years almost reaching the number of Ka band radars deployed within the



ARM program. Due to differences between radar systems (e.g. radar beam width) it is not clear whether the settings found within ARM are directly transferable to the MIRA systems. In this study, the requirements for high quality radar Doppler spectra are explored for this new class of operating radars. The developed strategies to obtain the optimal settings can also be applied to any other radar system.

- 5 The early detection of drizzle using the radar Doppler spectra skewness is used here as the target for this optimization. While the presented methodology can be applied also to other microphysical processes, we selected drizzle development because it is one of the most intensively studied applications with higher radar moments. Some of the relevant radar parameters necessary to capture signatures of drizzle development are hardware dependent. For example, a large radar beam width will increase the influence of dynamical broadening effects like turbulence or spectral artifacts caused by partial beam filling. Problems of
 10 partial beam filling will also occur when the observed cloud is thin with respect to the pulse length (Uttal and Kropfli, 2001). Other parameters, like the integration time or spectral resolution, can be adjusted by the user and their impact on moments estimation in the context of drizzle detection was never assessed before.

The integration time specifies how many initially derived Doppler spectra are temporally averaged by the radar processing software to a single spectrum which is then stored and from which all further radar moments are derived. A longer integration
 15 time reduces data storage space and helps to improve the signal to noise ratio. At the same time, longer integration time results in smearing of microphysical signatures due to small scale turbulence and radar-resolved vertical air motion (Kollias et al., 2007a). The second critical parameter is the spectral resolution. The spectral resolution of the Doppler velocity is defined by

$$\Delta v = \frac{2v_N}{n_{\text{fft}}} \quad (1)$$

where v_N is the Nyquist velocity and n_{fft} is the length of the discrete Fast Fourier Transform (FFT) used to produce the
 20 Doppler spectrum. A too coarse spectral resolution might introduce biases in the moment estimation (uncertainties in discrete integration) and can also be responsible for loss of specific microphysical signatures (e.g. the very narrow peak of super-cooled liquid water in mixed-phase clouds). As can be seen in Table 1 the most widely used settings in the MIRA community for integration time and spectral resolution are 10 s and 0.08 ms^{-1} ($n_{\text{fft}} = 256$), respectively. In contrast, the majority of cloud radars operated within the Atmospheric Radiation Measurement (ARM) program use a much smaller integration time of 2
 25 s and a finer spectral resolution of 0.03 ms^{-1} ($n_{\text{fft}} = 512$) (Kollias et al., 2007a). Moreover, different antenna beam widths, respectively 0.3° and 0.6° are used in ARM and MIRA communities.

Considering the number of researchers working with both systems, it is important to address the question whether such differences in radar hardware and sampling strategy affect the portability of retrievals algorithms from one cloud radar system to another. In order to answer this question, we recorded raw radar data (hereafter called I/Q data) of two shallow liquid clouds
 30 at the Jülich Observatory for Cloud Evolution (JOYCE) (Löhnert et al., 2015) which is described in Section 2. The clouds have been identified by the Cloudnet categorization algorithm (Illingworth et al., 2007) to be a non drizzle and drizzle case, respectively. The collected I/Q data allowed us to derive Doppler spectra and moments with different integration times and spectral resolutions. In this way, we were able to study the sensitivity of reflectivity, mean Doppler velocity, spectral width, and skewness to the different settings based on the identical raw data (Section 3). We further compared the observed sensitivities



with results from experiments performed with a radar Doppler spectrum forward simulator assuming a range of dynamical and microphysical conditions that match retrieved turbulence parameters and our observed distribution of reflectivity and skewness and we used the simulator also to assess the impact of different radar beam widths. Concluding remarks are given in Section 4.

2 Data and Methodology

5 2.1 Cloud Radar

We analyzed two case studies of shallow liquid clouds observed at the Jülich Observatory for cloud evolution (JOYCE) (Löhnert et al., 2015), equipped with a Ka-band MIRA Doppler cloud radar (hereafter called JOYRAD-35) (Fig. 1). Due to its high sensitivity it is well suited for the study of thin, low reflectivity clouds such as non-drizzling and drizzling stratocumulus clouds which are often observed over JOYCE. JOYRAD-35 transmits linear polarized wave at 35.5 GHz and simultaneously receives the co- and cross- polarized backscattered signal. The antenna beam width is 0.6° and the range resolution is 30 m. Observations in zenith mode are usually obtained at JOYCE with an integration time of 1 s, and a 256 point FFT for generating the Doppler spectrum. JOYRAD-35 allows to change the number of FFT points from 256, 512, up to 1024. According to Eq. (1) and given the Nyquist velocity of 10.625 ms^{-1} , we were able to realize spectral resolutions ranging from 0.08 ms^{-1} (standard settings) up to 0.02 ms^{-1} .

15 2.2 Raw Data Processing and Moment Estimation

The JOYRAD-35 raw radar data processing is similar to the method described in Doviak and Zrníc (2014). The raw I/Q time series are converted into Doppler spectra from which the final Doppler spectrum is generated by averaging the raw spectra over a given integration time. This procedure is exemplary illustrated in Figure 2 only for the I signal for a thin liquid cloud described in the following sections. Raw I/Q data are usually not stored because of their immense data volume (a raw file containing 1 min of I/Q observations results in a file of 1.2 GB size). For this study we recorded the original I/Q data in order to analyze the sensitivity of the spectra and their moments to different n_{fft} and integration times ΔT while using identical raw data. However, due to data storage limitations we had to restrict the maximum length of the recorded data to four minutes.

The raw I/Q data were processed using $n_{\text{fft}} = 256, 512, 1024$ and three different integration times $\Delta T = 0.4 \text{ s}, 2 \text{ s}, 10 \text{ s}$. A different number of radar Doppler spectral averages was used for different n_{fft} in order to achieve the final Doppler spectrum for one of the selected ΔT (Table 4). Only spectra within the cloud boundaries as identified by the Cloudnet classification algorithm were analyzed. We used the same procedure as described in Hildebrand and Sekhon (1974) to estimate the radar Doppler spectra noise floor (mean and peak value). The radar moments were calculated by subtracting peak noise level from the averaged spectrum $\hat{S}(v)$ of the Doppler velocity v (in ms^{-1}) using the following expressions (e.g. Kollias et al., 2011a). First, the radar Doppler spectrum \hat{S} is converted from SI-units to S in $\text{mm}^6 \text{ s m}^{-4}$ with

$$30 \quad S(v) = 10^{18} \frac{\lambda^4}{|K_w|^{2\pi^5}} \hat{S}(v), \quad (2)$$



where $|K_w|^2$ is related to the refractive index of liquid water and λ is the radar wavelength in m. Commonly, $|K_w|^2$ is fixed to 0.93 (default value in MIRA processing).

Then, the equivalent radar reflectivity factor Z_e (zeroth moment, hereafter called reflectivity) in $\text{mm}^6 \text{m}^{-3}$ can be obtained with

$$Z_e = \int_{-v_N}^{v_N} S(v) dv \quad (3)$$

The mean Doppler velocity V_d in ms^{-1} is related to the first moment of the Doppler spectrum and defined as

$$V_d = \frac{1}{Z_e} \cdot \int_{-v_N}^{v_N} S(v) \cdot v dv. \quad (4)$$

Z_e represents the integral of the spectrum within the Nyquist velocity range. For Rayleigh scatterers, Z_e is equal to the reflectivity factor Z which is defined as the sixth moment of the drop size distribution (DSD) (Doviak and Zrnic, 2014). V_d is the reflectivity weighted mean velocity of the scattering particles relative to the radar. The radar spectral width in ms^{-1} is related to the second moment of $S(v)$ and defined as

$$S_w = \sqrt{\frac{1}{Z_e} \cdot \int_{-v_N}^{v_N} S(v) \cdot (v - V_d)^2 dv} \quad (5)$$

S_w represents the variance of the hydrometeor's motions. In absence of vertical air motion and turbulence, it only depends on the variability of terminal fall velocities within the radar volume and hence reflects the width of the DSD. Air motion can additionally broaden the spectrum and enhance S_w . A comprehensive description of broadening effects can be found in Doviak and Zrnic (2014).

The skewness S_k (dimensionless) of the Doppler spectrum is related to the third moment and describes the asymmetry of a given spectrum with respect to an ideal Gaussian shape.

$$S_k = \frac{1}{Z_e \cdot (S_w)^3} \int_{-v_N}^{v_N} S(v) \cdot (v - V_d)^3 dv \quad (6)$$

The sign of S_k depends on the sign convention adopted for the Doppler velocity. In this study, we adopted the convention of velocities being positive when moving towards the radar (downwards) which results in positive S_k values occurring when the spectrum shows an asymmetry to the right of the main peak. S_k as well as S_w are of particular interest for studying drizzle growth as revealed by former studies (Luke and Kollias, 2013; Kollias et al., 2011a, b).

2.3 Non drizzle and Drizzle Dataset

Two four minutes long I/Q time series from stratiform thin liquid clouds classified by the Cloudnet algorithm to be non drizzle and drizzle clouds, respectively were analyzed. The non drizzle case was recorded at JOYCE on 20 November 2014 between



12:00:00 and 13:00:00 UTC. The thin cloud layer was located between 300 m and 500 m above ground (Fig. 3). The liquid water path (LWP) derived from the collocated microwave radiometer only reached values up to 50 gm^{-2} . The time-height structure of S_w processed for the three different spectral resolutions (n_{fft}) and integration times (ΔT) is shown in the lower panels of Figure 3. Longer integration time smooths the microphysical and dynamical structures and results in an increase of S_w with longer ΔT . On the other hand, the spectral resolution has only a minor effect on the derived S_w . Also the effects of the different settings on the reflectivity and S_k field (not shown) are small.

The time series of a drizzle event was recorded on 24 June 2015 between 09:00:00 and 10:00:00 UTC (Fig. 4). The drizzling cloud first appeared during nighttime and its cloud boundaries ranged between 700 m and 1000 m. The Cloudnet classification identified this cloud as drizzling until approximately 09:00 UTC. When the I/Q data were recorded, drizzle was ending over JOYCE and the cloud disappeared within the following hours. LWP decreased from the highest values observed in the morning (200 gm^{-2}) to values of 93 gm^{-2} during the I/Q collection period.

Compared to the non drizzle case (Fig. 3) the presence of drizzle is clearly indicated in the 10 dB larger reflectivities and enhanced positive S_k up to 1.5 (Fig. 4). Unlike the non-drizzling case, particularly the higher radar moments like S_k are now revealing larger sensitivity to the radar settings. The spectral resolution (as indicated by the changing n_{fft}) has a relatively small effect on the temporal-spatial structure of S_k . The variability of S_k appears to be best captured with 2 s integration time while extreme values and structure is lost when using 10 s integration time. A smaller value of 0.4 s seems not to provide more structure but rather to increase the noise. Both in the non drizzle and drizzle case, a much larger "smearing effect" when changing from 2 s to 10 s averaging time compared to moving from 0.4 to 2 s is found. While this effect is certainly connected to the scales of variability of the underlying cloud structures, it is noteworthy because the majority of cloud radars across Europe use 10 s integration time while the typical integration time for cloud radars at the ARM sites is 2 s. One question we aimed to address with this study is whether this is relevant only for specific case studies or whether such discrepancies in radar settings might also have implications on the derived radar moment statistics, which may affect the quality of evaluating drizzle parametrizations in numerical models.

2.4 Radar forward simulator

The observed radar Doppler spectra are affected by the underlying microphysics but also by dynamical effects such as turbulence. In reality, a complete separation of both effects is often a challenging task (Tridon and Battaglia, 2015). The limitations for storing the large amounts of I/Q raw data also limited the total observed time of drizzle clouds. To analyze the effects of dynamics and microphysics separately but also to investigate whether the observed drizzle signatures are consistent with commonly used assumptions about drizzle microphysics, we performed forward simulations of radar Doppler spectra and their corresponding moments using the radar forward simulator included in the Passive and Active Microwave radiative TRANSfer (PAMTRA) framework (Maahn, 2015). The radar operator implemented in PAMTRA is similar to the radar simulator described in (Kollias et al., 2014). Mie scattering (Mie, 1908) is used to estimate the backscattering properties, then the approach of Khvorostyanov and Curry (2002) is used to assign the corresponding fall velocity to every size bin. Finally, turbulence is convoluted and noise is applied in agreement with the MIRA characteristics (Zrnic, 1975). The moments of the synthetic



Doppler spectra are derived in the same way as for the observations. Input variables for PAMTRA include the DSD of cloud and drizzle populations, radar instrument parameters like antenna beam width, n_{ft} , and ΔT as well as vertical air motion and Eddy Dissipation Rate (EDR).

3 Results and Discussion

5 In this section the impact of different integration times and spectral resolutions on the derived radar moments using the collected I/Q datasets for non drizzle and drizzle clouds is analyzed. The observations are subsequently compared to the radar forward simulations in order to assess the impact of different n_{ft} and ΔT on identifying drizzle growth signatures under different turbulence conditions.

3.1 Impact of Integration Time and Spectral Resolution

10 The impact of different integration times on the radar moments is illustrated in Fig. 5. Time series of the four radar moments are shown for the drizzle case (Fig. 4) close to cloud top at 1007 m and close to cloud base at 806 m. The selection of the radar integration time impacts the higher moments of the radar Doppler spectrum stronger. In addition, the impact close to cloud base is higher than at cloud top which can be explained by the wider DSD at the lower regions of the cloud where the microphysical processes of autoconversion and accretion will result in larger drizzle particles and a wider drizzle DSD. The
 15 integration time has little effect on the recorded radar reflectivity values. The Z_e absolute differences between values derived with different integration times are smaller than 2 dB and as expected, longer integration times reduce the variability of Z_e (standard deviation of the time serie of Z_e at 0.4 s, 2 s and 10 s is reduced respectively from 1.0 dBz to 0.6 dBz and 0.56 dBz). The small dependency of the Z_e field on the integration time is consistent with the incoherent nature of the return power measurements and the lower frequency (longer wavelength) variability of the radar reflectivity field compared to the dynamical
 20 field.

Larger deviations are found for V_d particularly between the 10 s and the two shorter integration times. While the differences at cloud top are relatively small, at cloud bottom V_d values obtained with 10 s integration time sometimes deviate up to 50 % from the values derived with 2 s and 0.4 s. This is due to the broader and more skewed spectra observed at cloud bottom in combination with more variable vertical motions. Furthermore, the spectrum width increases with longer integration times
 25 because narrow individual spectra which are shifted due to vertical air motions are averaged together; this also results in a more Gaussian shape of the average spectrum and hence skewness values are closer to zero (Luke and Kollias, 2013). It is noteworthy that for all radar Doppler spectra moments only small differences are found between the 2 s and 0.4 s integration time but much larger differences when using 10 s. At least for drizzle studies, integration times equal or shorter than 2 s should be preferred for capturing small-scale vertical motions and to ensure high quality of higher moments (S_w , S_k) of the Doppler spectrum.
 30 Moreover, the non drizzle case is used as a benchmark for the statistical variance of the radar measurements. In non-drizzling conditions, the radar Doppler spectrum is dominated by turbulence (Kollias et al., 2001) and thus, the impact of microphysics on the shape of the radar Doppler spectrum can be neglected. For this reasons, the uncertainty due to instrumental noise and air



motions can be provided in these conditions. From the measurements, the uncertainty derived from the skewness time series collected in the non drizzling cloud using 2 s integration time and spectral resolutions of 256, 512 and 1024 ranges between 0.389 and 0.369 with a mean value over the three cases of 0.379.

For relatively narrow spectra, as they are found in clouds with no or little drizzle production, the spectral resolution might be of relevance for the quality of the derived moment estimates. The spectral resolution could affect the quality of integral values such as reflectivity if a narrow spectrum – e.g. due to cloud droplets – is only resolved with a few spectral bins. A larger impact is expected for higher moments where the spectral shape becomes important and hence spectral resolution potentially smoothes out spectral features. In order to investigate these potential effects of spectral resolution on the different moments, we derived the Doppler spectra for all heights with 256, 512, and 1024 n_{fft} . The integration time for all n_{fft} was kept constant (2 s) to ensure that the spectra are based on identical time series of raw I/Q data and hence they contain identical information about dynamics and cloud microphysics. The bias and standard deviations (STD) of the scatter plots (Fig. S1 and S2 in the supplemental information) of $n_{\text{fft}} = 256$ versus 512 and 512 versus 1024 for the drizzle and the non drizzle case are summarized in Table 5. In summary, the impact of different spectral resolutions is surprisingly small compared to the natural variability of the various moments shown in Fig. 5. Biases and STD are slightly larger for the non drizzle case while differences around 0.3 dB for reflectivity can still be considered negligible for most applications. The larger deviations in the non drizzle case are attributed to the insufficiently resolved narrow spectra which lead to uncertainties in the estimate of the integral and spectral shape. For example, narrow non-drizzling cloud spectra are often represented by only few spectral bins when using a spectral resolution of 0.08 ms^{-1} ($n_{\text{fft}} = 256$) as it is widely used by MIRA systems (Tab. 1). Such a coarse resolution also affects higher moments like S_w and S_k . In the drizzle case, the spectra are broader and sufficiently resolved even with the coarsest spectral resolution.

The observed normalized probability density functions of all radar Doppler spectra moments for the three different integration times, and three n_{fft} for the drizzling case (Fig. 6) and for the non-drizzling case (Fig. S3 in the supplementary material) were assessed in order to closer examine the reasons for the mismatches. Because Table 5 already showed that the impact of different spectral resolutions is rather limited, discussion will mainly be focused on the impact of integration time. For the non drizzle case, the distributions mainly show an expected increase in radar sensitivity and a shift in S_w towards larger values with longer integration time. The low spectral width and the low signal-to-noise ratio of the non drizzle spectra causes the spectra to be rather noisy. Higher moments like S_k are more affected by the low signal-to-noise conditions, which explains the relatively broad S_k distribution. Our analysis focused mainly on the drizzle case shown in Fig. 6 in order to capture the effects that the two radar settings can have in presence of drizzle forming. Moreover, higher signal-to-noise conditions during drizzling conditions were expected to limit the influence of noise on the derived distributions. The presence of drizzle is visible in the distributions of radar moments: in comparison to the non drizzle case, Z_e values are increased by about 10 dB and also the mean Doppler velocity peaks at about 0.25 ms^{-1} . Furthermore, the distribution of higher moments shows typical signatures of drizzle with S_w values larger by 0.6 ms^{-1} compared to the non drizzle observations (see Table 7). The skewness values reveal the typical transition from almost zero values in the non drizzle case to positive values with a mean around 0.25, indicating an asymmetry of the spectrum towards larger fall velocities due to larger drizzle particles; these signatures are in general agreement with former studies (e.g. Kollias et al., 2011a). Integration time as well as spectral resolution seem to have negligible



influence on the distributions of Z_e and V_d . The S_w values are considerably increased for the 10 s integration time while the shift is small for the two smaller integration times. The mean of the S_k distributions slightly decreases due to longer integration times (Table 7) which can be again explained by the more Gaussian shape of the spectra obtained using a longer integration time. Interestingly, particularly the largest values found in the positive S_k region are decreasing for longer integration times.

5 A similar but weaker effect can be found for the most positive V_d which we explain with relatively narrow regions within the cloud layer that already developed a larger amount of drizzle compared to the surrounding cloud layer. In the light of early detection of drizzle onset regions, a 10 s integration time seems to be insufficient. The differences obtained in the skewness distributions can have impacts on the ability to detect positive skewness signals induced by drizzle. Luke and Kollias (2013) showed S_k time series where the highest observed values of skewness reach up to 1.5. A reduced ability in detecting such

10 extremes values due to longer integration times (for example with 10 s integration time, the maximum value observed is 1) can affect the potential to disentangle the low frequency variability induced by the microphysics and the high frequency variability due to noisiness and beam filling issues. Finally, the coarsest spectral resolution using $n_{\text{fft}} = 256$ is found to be sufficient to properly capture the typical signatures of drizzle onset.

3.2 Comparison with Radar Forward Simulations

15 In this section we compare the results found in our observations with radar forward simulations using PAMTRA (see Sec. 2.4) to better understand drizzle signatures and compare the effects of distinct radar parameters. The main goal of the simulations was to derive a range of possible microphysical and dynamical conditions which lie within the observed range of radar moments. This helped us prove that the observed differences due to radar settings are significant for identifying drizzle onset. In addition, it helped us overcome one main limitation of our observations: that they are based on relatively short time periods. The

20 simulations further allowed us to separately analyze the effects of turbulence and vertical air motion, which are input parameters for PAMTRA, from the microphysics when observed with different n_{fft} and ΔT . For the cloud droplet and drizzle components we assumed a log-normal DSD of the form

$$N(D) = \frac{N_0}{\sqrt{2 \cdot \pi \sigma D}} \exp \left[-\frac{\log\left(\frac{D}{D_0}\right)^2}{2\sigma^2} \right] \quad (7)$$

where N_0 is the total number concentration (cm^{-3}), D_0 is the median diameter in m which is related to the effective diameter

25 (D_{eff}) by $D_0 = D_{\text{eff}} \exp \left[-\frac{5}{2}\sigma^2 \right]$ (Miles et al., 2000). The effective diameter is connected to the effective radius R_{eff} by the relation $D_{\text{eff}} = 2 \cdot R_{\text{eff}}$. Similar to (Miles et al., 2000) we used for cloud droplets an effective radius $R_{\text{eff},c} = 5.4 \mu\text{m}$, $\sigma_c = 0.35$ and total number concentration $N_0 = 300 \text{ cm}^{-3}$. With these assumptions, we obtained a liquid water content (LWC) for the cloud droplet component of $LWC_c = 0.137 \text{ gm}^{-3}$. This LWC is very close to the LWC of 0.133 gm^{-3} which we obtained in

30 the drizzle case when we divided the average LWP obtained by the MWR by the average geometrical thickness of the cloud layer. We assumed that the LWC due to drizzle (LWC_d) is much smaller than LWC_c which is a common assumption in simulations of drizzle onset. In Frisch et al. (1995) the LWC ratio derived from the standard parameters used to discriminate between cloud and drizzle is 5%, while in O'Connor et al. (2005) drizzle LWPs are often 2 orders of magnitude lower than



cloud LWP. For the simulations we varied the LWC ratio (r_{LWC}) defined as $r_{LWC} = \frac{LWC_d}{LWC_c}$ between 0.1 and 5%. For the log-normal drizzle DSD we used $\sigma_d = 0.35$ (Frisch et al., 1995) and varied the drizzle effective radius $R_{eff,d}$ from 10 μm to 60 μm . The drizzle number concentration N_d was then calculated based on the selected r_{LWC} . The DSDs for cloud droplets and drizzle are shown in Figure 7.

- 5 We derived distributions of Eddy Dissipation Rate (EDR) and V_d for the one hour period before the I/Q recording in order to obtain observational constraints for turbulence and vertical air motion needed as input to the radar forward simulations. EDR values were derived with an FFT method of V_d time series similar to the method described in Borque et al. (2016) which revealed a mean EDR of $3 \times 10^{-4} \text{ m}^2\text{s}^{-3}$ and a standard deviation of $1.3 \times 10^{-4} \text{ m}^2\text{s}^{-3}$. We also used the observed statistics of V_d as a first order approximation for the vertical air motion. We derived a mean value of 0.43 ms^{-1} and a standard deviation
- 10 of 0.39 ms^{-1} ; due to the non-negligible terminal velocity of the drizzle component, the true air motion is likely to be smaller.

Simulated spectra respectively for $r_{LWC} = 2 \%$ and $R_{eff,d} = 20 \mu\text{m}$ and $r_{LWC} = 0.5 \%$ and $R_{eff,d} = 30 \mu\text{m}$ (to simulate different stages of drizzle onset), and EDR representing the mean ($3 \times 10^{-4} \text{ m}^2\text{s}^{-3}$) and largest values ($5 \times 10^{-3} \text{ m}^2\text{s}^{-3}$) observed are shown exemplary in Figure 8. We interpret the first scenario as an early drizzle onset and the second scenario as a more developed stage of drizzle. For $R_{eff,d} = 20 \mu\text{m}$, the contribution of the drizzle DSD to the convoluted spectrum is

15 dominated by the cloud droplet peak even for low turbulence conditions. When the $R_{eff,d}$ is increased to 30 μm , the drizzle contribution becomes stronger and causes the spectrum to become positively skewed. Increasing the EDR in general leads to a smoothing and symmetrical broadening of the spectrum but the overall asymmetry due to drizzle is still clearly visible. A comparison of our simulations with observed spectra from regions where we assume no-drizzle and drizzle growth (Fig. 8) shows an overall good agreement in terms of spectral shape, Z_e , and S_k .

- 20 In order to take the effects of turbulence and changes in vertical velocity on the distribution of the Doppler spectra moments into account, we utilized the same microphysical scenarios described above. For each scenario, we run 1000 PAMTRA simulations choosing randomly the noise and a pair of values of EDR and vertical air motion (V_d) based on the observed distributions. In this way, we derived for each simulated spectrum statistically plausible air motion conditions (turbulence and vertical wind) which we expect to be close to the ones observed. The simulations were repeated for the three n_{fft} and ΔT in order to derive
- 25 distributions of radar moments similar to our observations (Fig. 6).

Statistical distributions of simulated moments of the convoluted spectra from cloud and drizzle droplets are shown in Fig. 9 and Fig. 10. Both simulation experiments produce reflectivities which are found among the highest Z_e values observed (Fig. 6). The simulated Z_e values lie in a narrow interval because we only assumed a single DSD of cloud and drizzle drops and only vary EDR and vertical air motion. The increasing variability with smaller averaging time and larger n_{fft} is related to the

30 increasing noisiness of the simulated spectra due to the small number of spectral averages. Very small effects of n_{fft} and ΔT are found for mean Doppler velocity which is similar to our observations (compare Fig. 9(d), (e), (f) and Fig. 10(d), (e), (f) with Fig. 6(d), (e), (f)). The simulated V_d distributions appear to be biased to positive velocities. This is not surprising considering that we assumed the distribution of V_d previous to our I/Q experiment as proxy for vertical air motion and that this distribution is biased towards larger positive velocities due to sedimentating drizzle drops. For S_w , the mean values of the distributions are

35 found to increase with larger integration times. The simulated increase closely matches for both simulations the observations



in Fig. 6; the $nfft$ seem to have a negligible effect on the S_w distributions in agreement with the observations. In contrast to the observations, the simulated S_k values are only positive and range up to 1.5. We address this effect to the use of the specific drizzle DSDs. These large positive values of simulated skewness with PAMTRA are a result of the long tail of the selected shape for the drizzle DSD. While this shape might be typical for mature drizzle distributions, the distribution is expected to be more narrow during the early stages of drizzle production (i.e. near cloud top). The absence of negative values is attributed to two factors. During heavy drizzle conditions a reversal of the sign of the S_k is expected, however, here this is not the case because the selected drizzle DSDs do not cause the drizzle spectrum to exceed the cloud droplet spectrum. The second factor is the absence of non-linear horizontal shear of the vertical air motion in the PAMTRA simulator. This is discussed in detail in Luke and Kollias (2013). Finally, low signal-to-noise conditions can increase the uncertainty of the measured radar Doppler spectra skewness and thus give rise to negative radar Doppler spectra skewness values, i.e. as those observed by JOYRAD-35.

Despite the missing negative S_k values in our simulations, smaller values of skewness using $20 \mu m$ effective radius for drizzle (Fig. 9) compared to the simulation for $R_{eff} = 30 \mu m$ (Fig. 10) are observed and a shift of the S_k distributions to larger values for smaller ΔT is found in both simulations.

This simulated effect is confirmed by observations particularly if we focus the analysis to cloud regions with spatio-temporal coherent positive skewness structures as shown in Figure 11. The distributions of skewness values for the three different integration times and a spectral resolution of $nfft = 256$ are shown in the upper panel of Fig. 11. A comparison with Fig. 10 reveals that the range of observed skewness values as well as the shifting of the peak and change in positive S_k extremes is very similar to the simulations.

Overall, the simulated distributions reveal – in agreement with observations – an only minor effect of $nfft$ on the S_k distributions. The distributions of simulated moments reproduce the main effects induced by integration time and spectral resolution on the moments estimations, confirming the choice of 256 $nfft$ length and 2 s integration time as optimal settings for drizzle detection.

We further analyze our findings for different microphysical situations as a function of assumed level of turbulence and the radar antenna beamwidth using a fixed integration time of 2 seconds (Fig. 12). At low turbulence conditions and very small r_{LWC} , the skewness shows very high values, which tend to decrease for larger r_{LWC} . In fact, increasing the liquid amount for drizzle generates a more pronounced drizzle peak which results in a spectrum more similar to a gaussian shape and less asymmetric than in the case of low r_{LWC} . The value of the skewness observed depends on whether the drizzle effective radius is large enough to introduce a sufficient asymmetry on the right of the cloud peak (see Fig. 8). If the effective radius of the drizzle is too small, the drizzle contribution is concealed by the cloud part and the skewness will be just slightly positive for increasing r_{LWC} . Figure 12 also shows that under low turbulence conditions the skewness signal generated by the presence of drizzle characterized by an effective radius of at least $20 \mu m$ is always greater than 0.4, which is the detection limit we estimated for the observations (see Subsection 3.1). This indicates that there is potential for the detection of drizzle onset of $20 \mu m$ effective radius within the cloud in presence of low turbulence. All skewness values are damped with respect to the ones derived in low turbulence conditions in presence of high turbulence (lower panel of Fig 12). Here, most of the expected skewness values are below the "noise threshold" and only drizzle of larger than $40 \mu m$ can be detected. Smaller beam widths



allows the detection of slightly higher skewness values in both turbulence conditions. The gain due to the beam width appears more evident for effective radii around $20 - 30 \mu\text{m}$, underlining the importance of this parameter for the accuracy of skewness estimation.

5 4 Conclusions

In this study we quantified how integration time and spectral resolution influence moment estimation in the specific context of liquid clouds and drizzle onset. Once certain radar settings (such as a long integration time) have been set by the user, a more detailed analysis is impossible and potentially interesting microphysical signatures are lost. Therefore, it is vital to carefully choose radar settings in order to establish high-quality datasets of cloud radar observations in drizzle clouds and to enable future comparisons of long-term datasets obtained with different radar systems and at different sites. This requires an optimal compromise between limiting the demands on data storage and conserving relevant microphysical information.

We analyzed consecutive zenith pointing radar observations for two case studies of liquid non drizzling and drizzling clouds. We found that in the specific context of liquid clouds and drizzle initiation longer integration times mainly modify spectral width and skewness leaving the other moments hardly altered. For drizzle applications, we found an uncertainty on skewness measurements to be on the order of 0.4.

Simulations performed with a radar forward simulator which allows to explicitly define the state of drizzle are in general agreement with observations. Spectral width is increased by longer integration times due to the broadening of the spectrum shape. In the observations this effect is attributed to turbulence and is confirmed by simulations. Skewness undergoes a reduction of the occurrence of larger values when longer integration times are used. From the simulations we conclude that both increase in S_w and reduction in S_k in case on the 10 s average can lead to significantly different microphysical interpretations with respect to drizzle water content and effective radius (Fig 12) compared to shorter integration times.

For the specific application of drizzle detection we found the integration time of 2 s to be an optimal compromise considering the turbulence-induced increase in S_w at longer integration times and the preservation of larger values of S_k . We also concluded that FFT lengths have a smaller impact on the moment estimations, and thus on the microphysical interpretation of the drizzle signal: 256 FFT length seems appropriate for moments calculation with no significant differences compared to 512 or 1024.

Moreover simulations provided additional insight into the microphysical interpretation of the skewness signatures observed: in low (high) turbulence condition, only drizzle bigger than $20 \mu\text{m}$ ($40 \mu\text{m}$) can generate skewness values above the noise level. Higher skewness values are also obtained in simulations when smaller beam widths are adopted compared to skewness values derived in the same conditions but with larger beam widths. Simulations also demonstrated the impact of the antenna beam width on the skewness measurements, showing the benefits of narrower beam widths.

In summary, this experiment presents a first step towards the optimal choice of radar parameter settings when retrieving drizzle parameters exploiting higher Doppler spectra moments. One clear limitation is the restriction to two short case studies due to the extremely large amount of data to be handled when working with IQ raw measurements. In this context, the agree-



Figure 1. Scanning Ka-band Doppler cloud radar JOYRAD-35 (JOYRAD-35 system) installed at the JOYCE site, Jülich, Germany. Technical specifications of the radar are provided in Table 2.

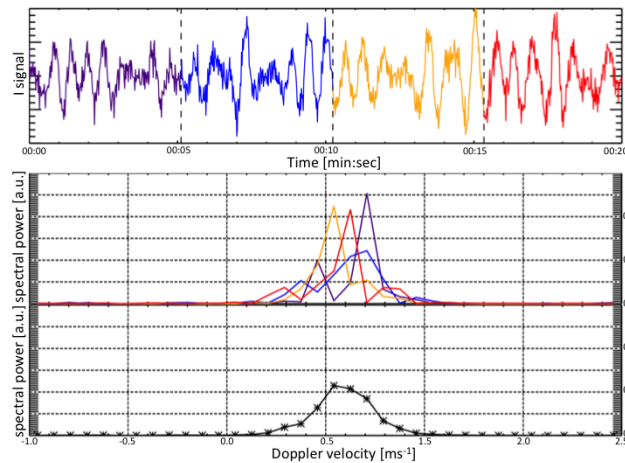


Figure 2. Illustration of the standard procedure for deriving radar Doppler spectra from raw I/Q time series (see also detailed description of the method in Doviak and Zrnic (2014)). The upper panel shows a time series of 1024 in-phase (I) samples (Q time series not shown); the different colors denote four 256 point long subsamples which are used in combination with the corresponding Q samples to perform a 256 FFT resulting in the raw Doppler spectra shown in the panel below. Each raw spectrum corresponds to an integration time of (0.0512 s). The lowest panel shows the average of the four raw spectra corresponding to a total integration time of 0.2 s.

ment between simulations and observations is even more striking, because the big amount of simulations performed (1000) underline and confirm what was observed during the short observation period. The developed methodology, showing how such requirements can be derived in general, will be to other cloud types and microphysical processes to verify how radar settings can impact the identification of spectral features like bi-modalities found in mixed-phase clouds due to the presence of super-cooled liquid water, ice, snow, and rimed particles (Shupe et al., 2004; Verlinde et al., 2013; Kalesse et al., 2015).

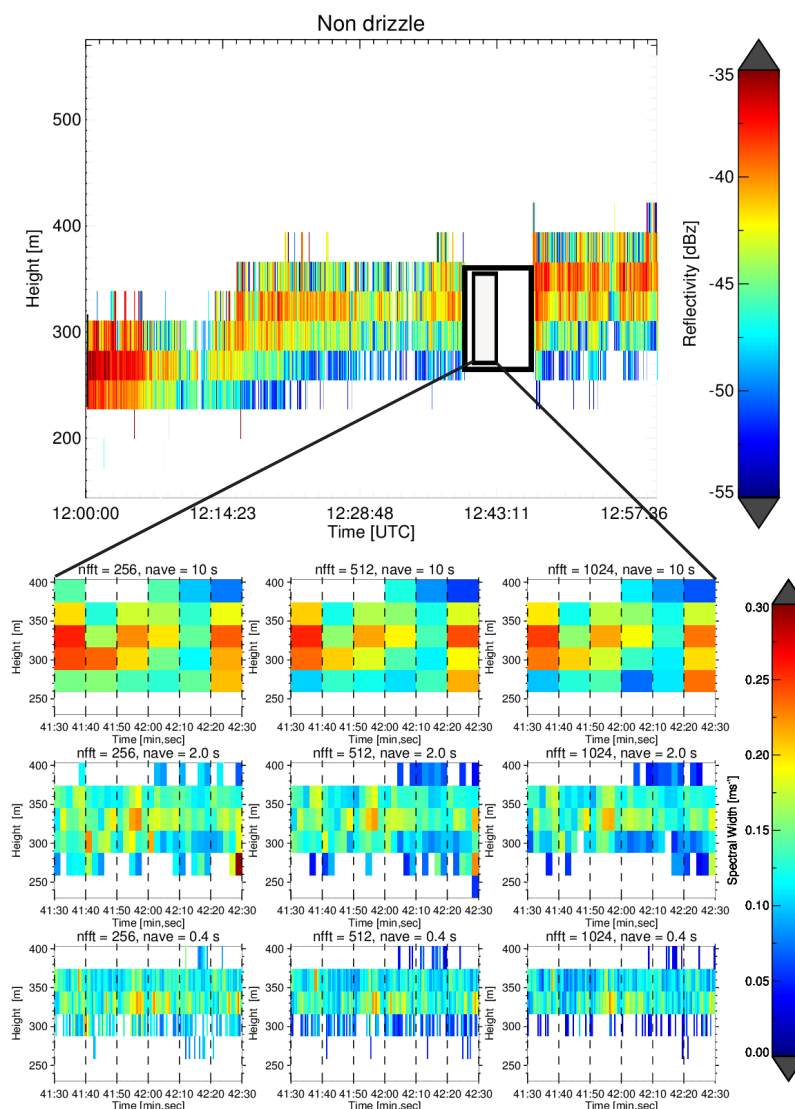


Figure 3. Time-height plot composite of reflectivity and spectral width for the non drizzle case on 20 November 2014. The larger upper panel shows the reflectivity for the entire one hour period obtained with standard radar settings of $nfft=256$ and $\Delta T=1$ s; the larger black box denotes the four minute time period of I/Q data recording. The lower subplots show time-height plots of a one minute time period (small black box) of spectral width for three different integration times (decreasing from top to bottom) and spectral resolutions (increasing from left to right).

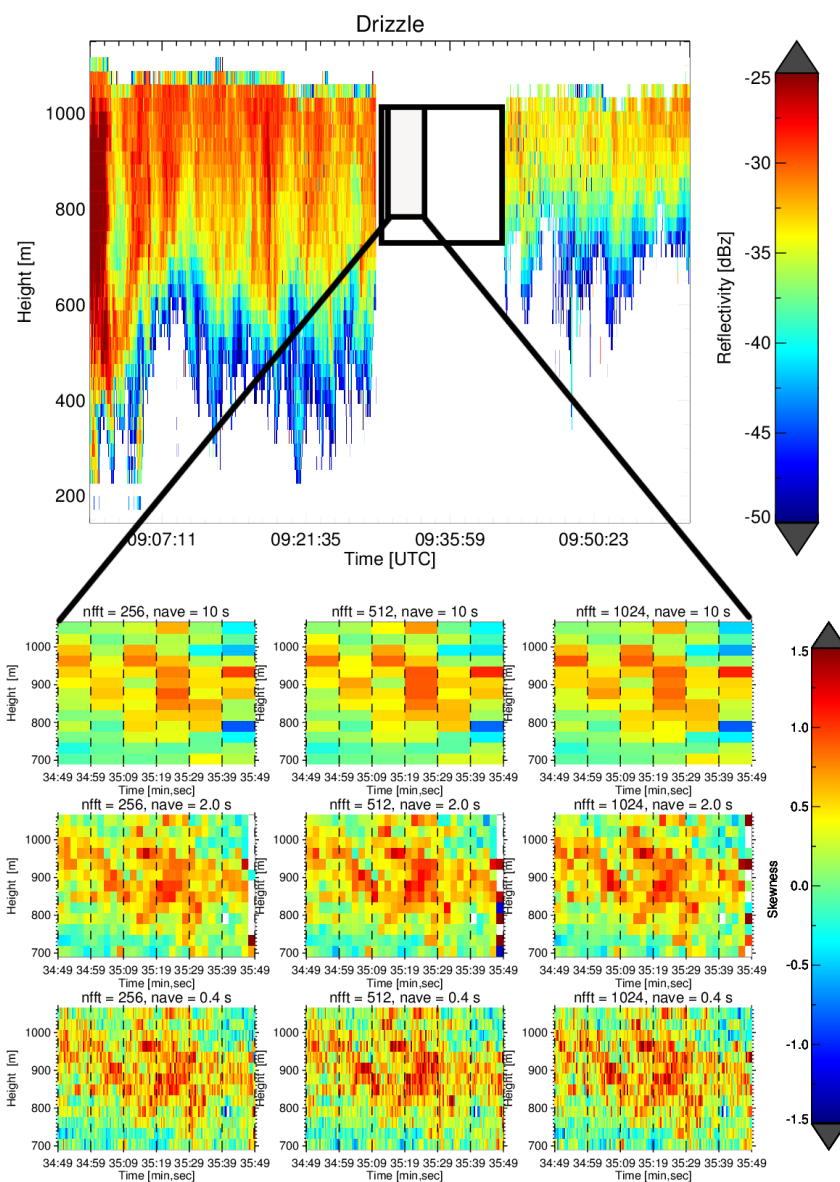


Figure 4. Similar to Figure 3 but for the drizzle case on 24 June 2015. For this case the subplots show skewness instead of spectrum width.

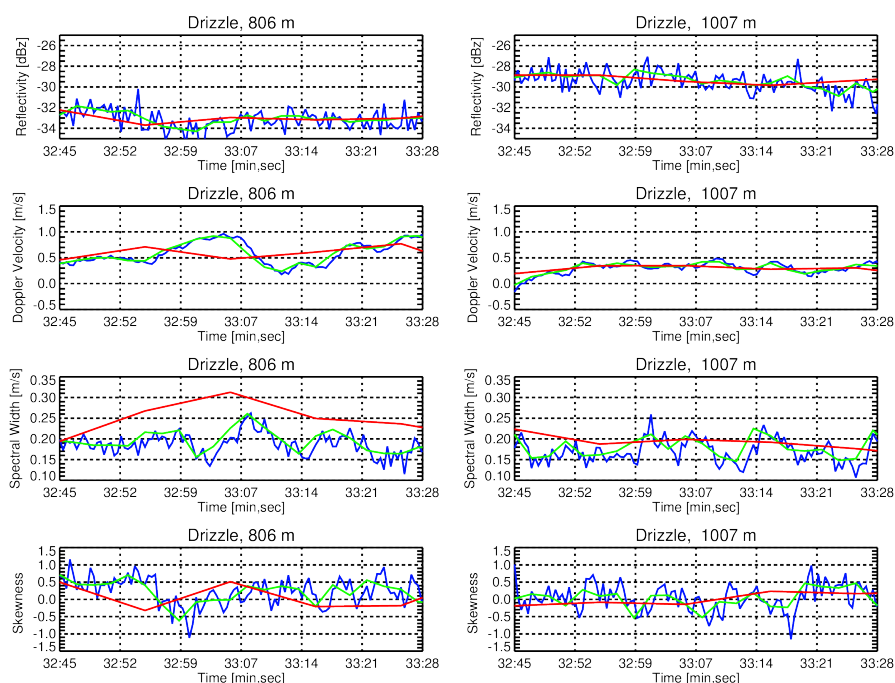


Figure 5. Example time series of the first four Doppler moments obtained from altitudes close to cloud top (right column) and close to cloud bottom (left column) for drizzle case on 24 June 2015 (see Fig. 4). Different colors correspond to different integration times of 10 s (red), 2 s (green), and 0.4 s (blue); n_{fft} for all time series is 512.

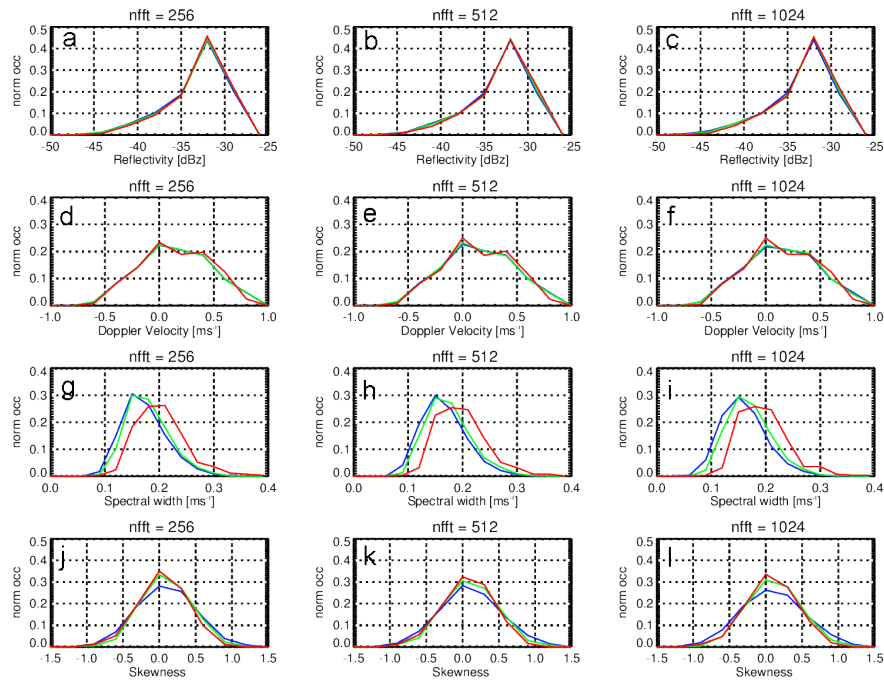


Figure 6. Distributions of radar moments for the drizzle case on 24 June 2015 (Fig. 4). The total number of values used for the different pdfs ranges between 252 for the 10 s integration time and 6174 for the 0.4 s integration time. Different colors in each plot correspond to different integration times of 10 s (red), 2 s (green), and 0.4 s (blue). The spectral resolution (nfft) increases from left to right; radar moments are from upper to lowest row: reflectivity (Z_e), mean Doppler velocity (V_d), Spectral Width (S_w), and Skewness (S_k).

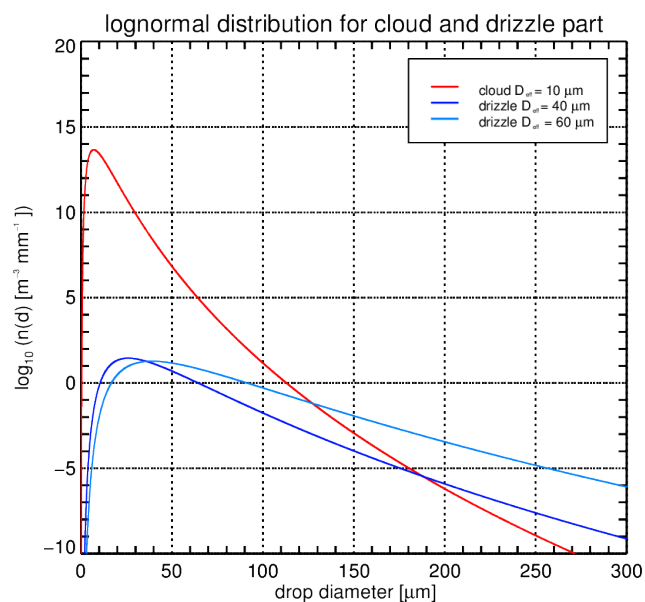


Figure 7. Drop size distributions used for radar forward simulations of the drizzle case. A single log-normal size distribution (red) is used for cloud droplets; for drizzle log-normal distributions with fixed $r_{LWC} = 0.5\%$ and two different effective diameters are used: $40\ \mu m$ (dark blue), $60\ \mu m$ (blue). The total number concentration N_d of the drizzle distribution is determined based on the other parameters according to Eq. (7).

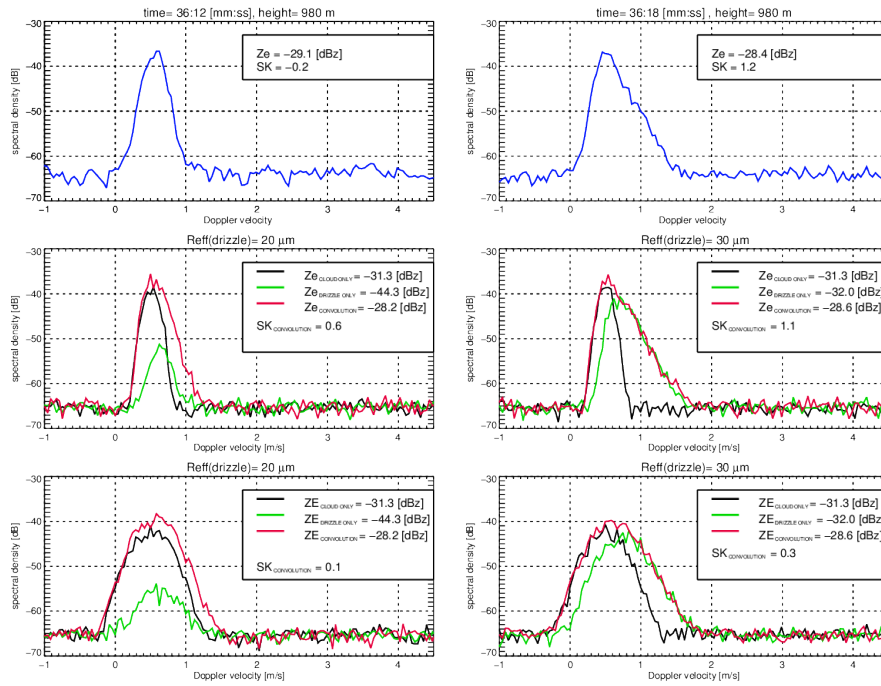


Figure 8. Comparison between simulated and observed spectra. Upper panels shows real Doppler spectra obtained during the drizzle-case for $n_{\text{fft}} = 512$ and $\Delta T = 2$ s in regions of early (left) and more mature drizzle development (right). The 4 lower panels show examples of simulated Doppler spectra for cloud droplets (black), drizzle (green) and cloud+drizzle drops (red) for a low EDR of $3 \times 10^{-4} \text{ m}^2 \text{ s}^{-3}$ (middle panels) and high EDR of $5 \times 10^{-3} \text{ m}^2 \text{ s}^{-3}$ (lower panels). The left column shows spectra for a log-normal drizzle DSD with effective radius of $20 \mu\text{m}$ while the right column is calculated with a drizzle effective radius of $30 \mu\text{m}$.

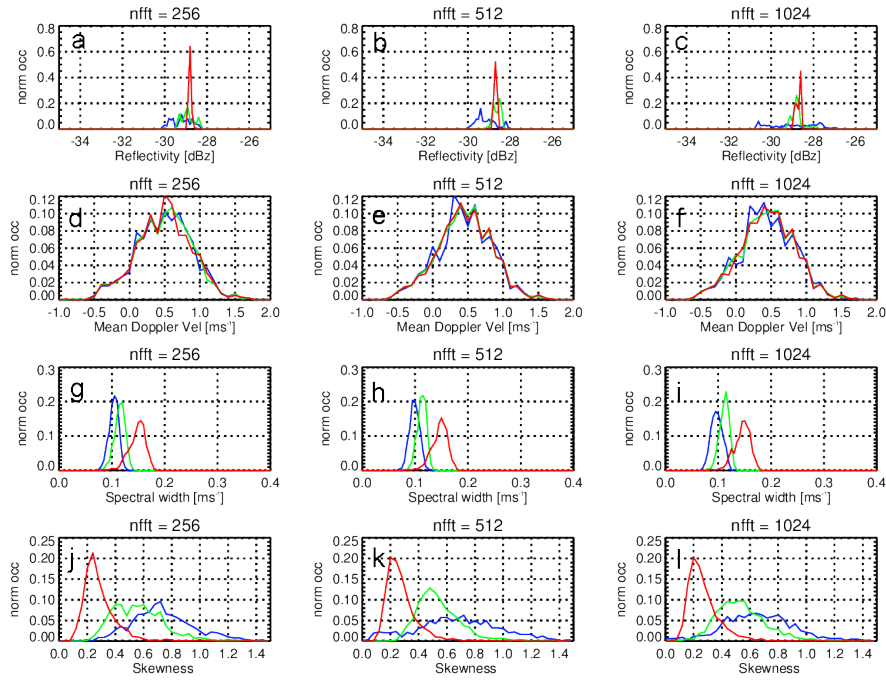


Figure 9. Distributions of simulated radar moments Z_e , V_d , S_w , S_k (from top to bottom) normalized by the total number of simulations ($N = 1000$) for cloud and drizzle droplets using $R_{eff,d} = 20 \mu m$ and $r_{LWC} = 2.0 \%$. The moments are derived for averaging times of 10 s (red), 2 s (green), and 0.4 s (blue) and different n_{fft} (increasing from left to right).

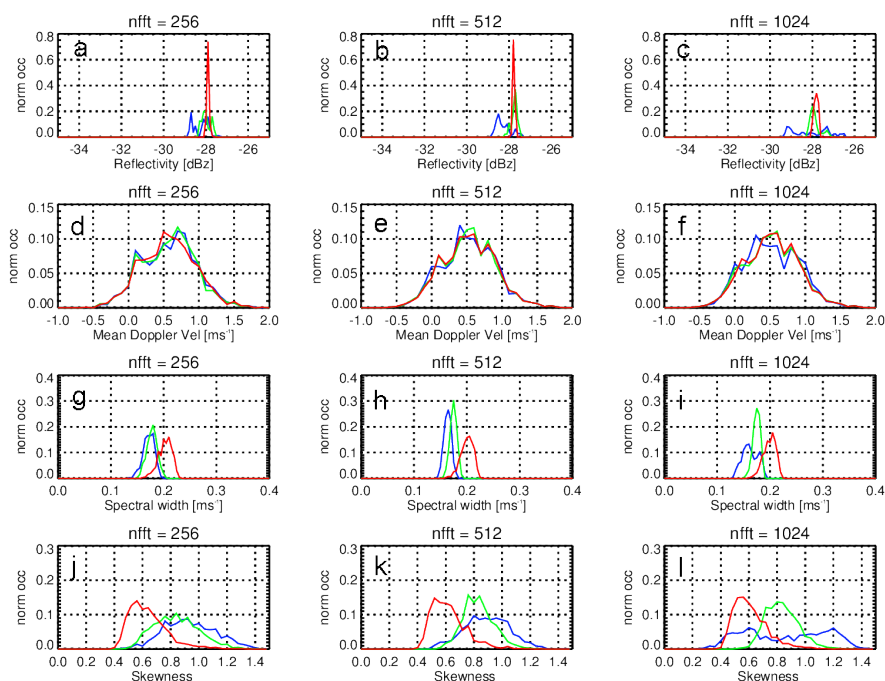


Figure 10. Similar to Figure 9 but using $R_{\text{eff,d}} = 30 \mu\text{m}$ and $r_{\text{LWC}} = 0.5 \%$.

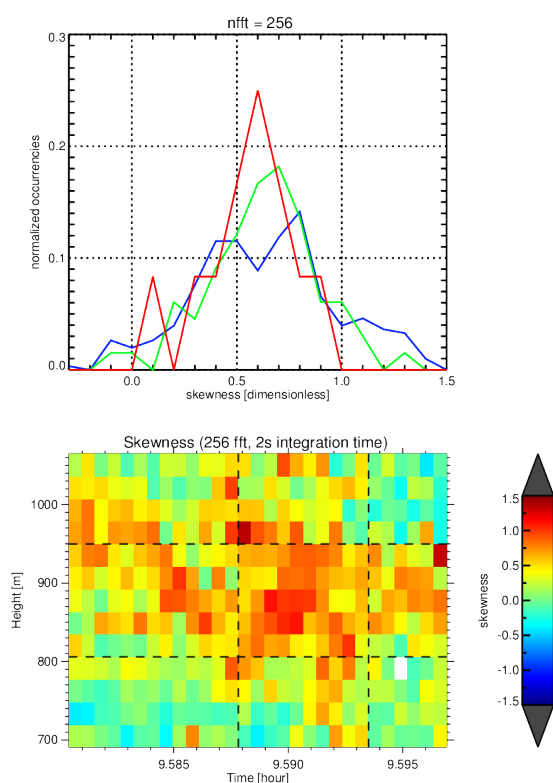


Figure 11. Selection of positive skewness values due to drizzle fingerprint in the observations from the case study of the 24 June 2015. Upper panel: distributions of skewness observed values derived using a spectral resolution of 256 and integration time of 10 s (red), 2 s (green) and 0.4 s (blue). Lower panel: box of positive skewness values selected for the analysis.

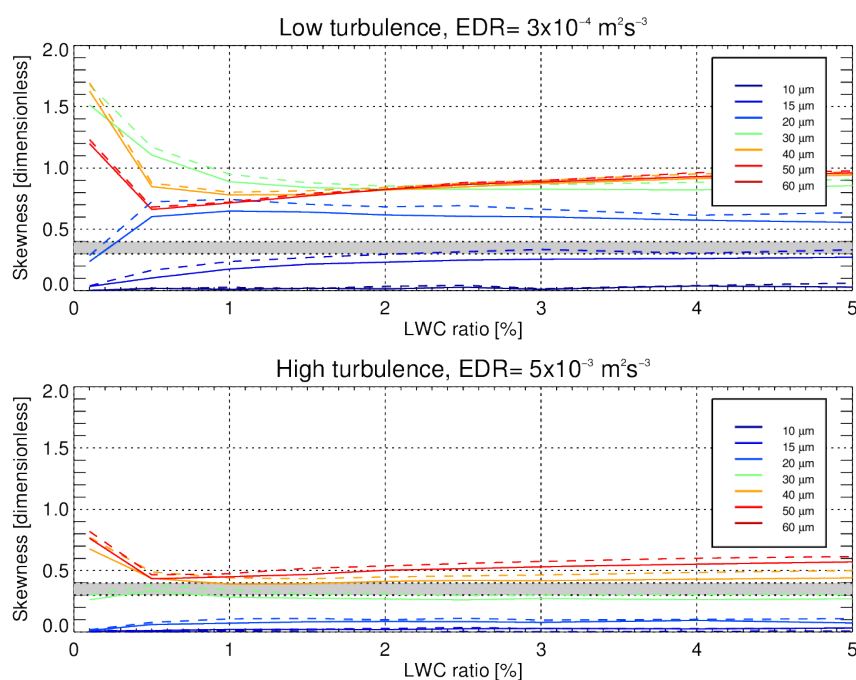


Figure 12. Skewness of the convoluted spectrum of cloud and drizzle drop size distributions as a function of r_{LWC} for different drizzle effective radii and low EDR (upper panel) and high EDR (lower panel). Simulations have been performed using 0.6° (solid line) and 0.3° (dashed line) radar beam widths. The grey bar represents the uncertainty of the skewness observations.



References

- Atlas, D., Srivastava, R., and Sekhon, R. S.: Doppler radar characteristics of precipitation at vertical incidence, *Reviews of Geophysics*, 11, 1–35, 1973.
- Borque, P., Luke, E., and Kollias, P.: On the unified estimation of turbulence eddy dissipation rate using Doppler cloud radars and lidars, *Journal of Geophysical Research: Atmospheres*, 2016.
- Doviak, R. and Zrnic, D.: *Doppler Radar & Weather Observations*, Academic press, 2014.
- Frisch, A., Fairall, C., and Snider, J.: Measurement of stratus cloud and drizzle parameters in ASTEX with a $K\alpha$ -band Doppler radar and a microwave radiometer, *Journal of the Atmospheric Sciences*, 52, 2788–2799, 1995.
- Görsdorf, U., Lehmann, V., Bauer-Pfundstein, M., Peters, G., Vavriv, D., Vinogradov, V., and Volkov, V.: A 35-GHz polarimetric Doppler radar for long-term observations of cloud parameters—Description of system and data processing, *Journal of Atmospheric and Oceanic Technology*, 32, 675–690, 2015.
- Gossard, E.: Measurement of cloud droplet size spectra by Doppler radar, *Journal of Atmospheric and Oceanic Technology*, 11, 712–726, 1994.
- Gossard, E. E., Snider, J., Clothiaux, E., Martner, B., Gibson, J. S., Kropfli, R., and Frisch, A.: The potential of 8-mm radars for remotely sensing cloud drop size distributions, *Journal of Atmospheric and Oceanic Technology*, 14, 76–87, 1997.
- Hildebrand, P. H. and Sekhon, R.: Objective determination of the noise level in Doppler spectra, *Journal of Applied Meteorology*, 13, 808–811, 1974.
- Illingworth, A., Hogan, R., O’connor, E., Bouniol, D., et al.: Cloudnet, *Bulletin of the American Meteorological Society*, 88, 883, 2007.
- Kalesse, H., Szyrmer, W., Kneifel, S., Kollias, P., and Luke, E.: Fingerprints of a riming event on cloud radar Doppler spectra: observations and modeling, *Atmospheric Chemistry and Physics Discussions*, 15, 28 619–28 658, 2015.
- Khvorostyanov, V. I. and Curry, J. A.: Terminal velocities of droplets and crystals: Power laws with continuous parameters over the size spectrum, *Journal of the atmospheric sciences*, 59, 1872–1884, 2002.
- Kollias, P., Albrecht, B., Lhermitte, R., and Savtchenko, A.: Radar observations of updrafts, downdrafts, and turbulence in fair-weather cumuli, *Journal of the atmospheric sciences*, 58, 1750–1766, 2001.
- Kollias, P., Clothiaux, E., Miller, M., Albrecht, B., Stephens, G., and Ackerman, T.: Millimeter-wavelength radars, *Bulletin of the American Meteorological Society*, 88, 1608, 2007a.
- Kollias, P., Miller, M. A., Luke, E. P., Johnson, K. L., Clothiaux, E. E., Moran, K. P., Widener, K. B., and Albrecht, B. A.: The Atmospheric Radiation Measurement Program cloud profiling radars: Second-generation sampling strategies, processing, and cloud data products, *Journal of Atmospheric and Oceanic Technology*, 24, 1199–1214, 2007b.
- Kollias, P., Rémillard, J., Luke, E., and Szyrmer, W.: Cloud radar Doppler spectra in drizzling stratiform clouds: 1. Forward modeling and remote sensing applications, *Journal of Geophysical Research: Atmospheres*, 116, 2011a.
- Kollias, P., Szyrmer, W., Rémillard, J., and Luke, E.: Cloud radar Doppler spectra in drizzling stratiform clouds: 2. Observations and micro-physical modeling of drizzle evolution, *Journal of Geophysical Research: Atmospheres*, 116, 2011b.
- Kollias, P., Tanelli, S., Battaglia, A., and Tatarevic, A.: Evaluation of EarthCARE cloud profiling radar Doppler velocity measurements in particle sedimentation regimes, *Journal of Atmospheric and Oceanic Technology*, 31, 366–386, 2014.



- Kollias, P., Clothiaux, E. E., Ackerman, T. P., Albrecht, B. A., Widener, K. B., Moran, K. P., Luke, E. P., Johnson, K. L., Bharadwaj, N., Mead, J. B., et al.: Development and Applications of ARM Millimeter-Wavelength Cloud Radars, *Meteorological Monographs*, 57, 17–1, 2016.
- Löhnert, U., Kneifel, S., Battaglia, A., Hagen, M., Hirsch, L., and Crewell, S.: A multisensor approach toward a better understanding of snowfall microphysics: The TOSCA project, *Bulletin of the American Meteorological Society*, 92, 613, 2011.
- Löhnert, U., Schween, J., Acquistapace, C., Ebell, K., Maahn, M., Barrera-Verdejo, M., Hirsikko, A., Bohn, B., Knaps, A., O'Connor, E., et al.: JOYCE: Jülich observatory for cloud evolution, *Bulletin of the American Meteorological Society*, 96, 1157–1174, 2015.
- Luke, E. P. and Kollias, P.: Separating cloud and drizzle radar moments during precipitation onset using Doppler spectra, *Journal of Atmospheric and Oceanic Technology*, 30, 1656–1671, 2013.
- Maahn, M.: Exploiting vertically pointing Doppler radar for advancing snow and ice cloud observations, Ph.D. thesis, Universität zu Köln, 2015.
- Maahn, M. and Löhnert, U.: Potential of higher order moments of the radar Doppler spectrum for retrieving microphysical and kinematic properties of Arctic ice clouds (in review), *Journal of Applied Meteorology and Climatology*, 2016.
- Maahn, M., Löhnert, U., Kollias, P., Jackson, R. C., and McFarquhar, G. M.: Developing and evaluating ice cloud parameterizations for forward modeling of radar moments using in situ aircraft observations, *Journal of Atmospheric and Oceanic Technology*, 32, 880–903, 2015.
- Mie, G.: Beiträge zur Optik trüber Medien, speziell kolloidaler Metallösungen, *Annalen der Physik*, 330, 377–445, doi:10.1002/andp.19083300302, <http://dx.doi.org/10.1002/andp.19083300302>, 1908.
- Miles, N. L., Verlinde, J., and Clothiaux, E. E.: Cloud droplet size distributions in low-level stratiform clouds, *Journal of the atmospheric sciences*, 57, 295–311, 2000.
- O'Connor, E. J., Hogan, R. J., and Illingworth, A. J.: Retrieving stratocumulus drizzle parameters using Doppler radar and lidar, *Journal of Applied Meteorology*, 44, 14–27, 2005.
- Shupe, M. D., Kollias, P., Matrosov, S. Y., and Schneider, T. L.: Deriving mixed-phase cloud properties from Doppler radar spectra, *Journal of Atmospheric and Oceanic Technology*, 21, 660–670, 2004.
- Tridon, F. and Battaglia, A.: Dual-frequency radar Doppler spectral retrieval of rain drop size distributions and entangled dynamics variables, *Journal of Geophysical Research: Atmospheres*, 120, 5585–5601, 2015.
- Uttal, T. and Kropfli, R. A.: The effect of radar pulse length on cloud reflectivity statistics, *Journal of Atmospheric and Oceanic Technology*, 18, 947–961, 2001.
- Verlinde, J., Rambukkange, M. P., Clothiaux, E. E., McFarquhar, G. M., and Eloranta, E. W.: Arctic multilayered, mixed-phase cloud processes revealed in millimeter-wave cloud radar Doppler spectra, *Journal of Geophysical Research: Atmospheres*, 118, 2013.
- Zrnic, D. S.: Simulation of weatherlike Doppler spectra and signals, *Journal of Applied Meteorology*, 14, 619–620, 1975.



Table 1. Current radar settings for operating MIRA METEK systems in the world.

| Location | Institution | Integration time ΔT [s] | n_{fft} | PRF [kHz] | V_N [ms ⁻¹] | Comments |
|---|---|---------------------------------------|-----------|--------------|------------------------------|---|
| Chilbolton (UK) | University of Leeds | 10 | 512 | 7.5 | 15 | |
| Cleveland (Ohio, USA) | NASA | 10 | 256 | 5 | 10 | |
| Galway (Ireland) | National University of Ireland (NUI) | 10 | 256 | 5 | 10 | |
| Hamburg (Germany) | Max Planck Institute (MPI) | 10 | 256 | 5 | 10 | |
| Iqaluit (Canada) | Environment Canada (EC) | 1 | 256 | 5 | 10 | |
| Jülich-JOYCE (Germany) | University of Cologne (IGMK) | 1 | 256 | 5 | 10.6 | |
| Karlsruhe, (Germany) | Karlsruhe Institute of Technology (KIT) | — | 256 | 5 | 10 | mainly used for campaigns |
| Kuopio (Finland) (before Helsinki and Sudankylä) | Finnish Meteorological Institute (FMI) | 10 | 512 | 5 | 10 | |
| Leipzig (Germany) | Leibniz Institute for Tropospheric Research (TROPOS) | 10 | 256 | 5 | 10 | 1 s resolution stored for 5 days, for special events (de- fined by the radar users) moment-data is re-processed with 1 s resolution |
| Lindenberg (Germany) | Deutscher Wetterdienst (DWD) | 10 | 256 | 5 | 10 | |
| Munich (Germany) | Ludwig-Maximilian Universität München (LMU) | 10 | 256 | 7.5 | 10 | |
| Potenza (Italy) | Consiglio Nazionale delle Ricerche: istituto di Metodologie per l'Analisi Ambientale (CNR-IMAA) | 10 | 256 | 5 | 10 | |
| Huancayo (Peru) | Laboratorio de Microfísica Atmos- férica y Radiación (LAMAR), Isti- tuto Geofísico del Perú (IGP) | 10 | 128 | 5 | 10 | |
| Zugspitze (Germany) | German Aerospace Center (DLR) | 10 | 256 | 5 | 10 | |



Table 2. Current radar settings for JOYRAD35 system at JOYCE, Juelich (DE).

| Parameter | Specification | Comments |
|--|----------------|---------------------------------------|
| Frequency | 35.5 GHz | corresponding to wavelength of 8.5 mm |
| Peak power (max) | 25 kW | |
| Average power | 24 W | |
| Pulse width | 200 ns | adjustable (100, 200, or 400 ns) |
| Pulse repetition frequency | 5 kHz | adjustable (5-10 kHz) |
| Minimum height | 150 m | full sensitivity above 400 m |
| Measuring range | 15 km | adjustable (7.5-30 km) |
| Range resolution | 30 m | adjustable (15, 30, or 60 m) |
| 3dB one way antenna beam width in the E and H planes | 0.6 deg | |
| Doppler velocity resolution | 0.025 m/s | depends on FFT length |
| Nyquist velocity | ± 10.6 m/s | |
| Maximum sensitivity at 5 km (integration 0.1 s) | -45 dBZ | |
| Calibration system accuracy | ± 0.5 dB | |
| Number of gates (with simultaneous stored raw data) | 500 | |
| Number of averaging spectra | 200 | adjustable (1-32768) |
| Manufacturer | Metek | |

Table 3. Minimum integration time to generate a single Doppler spectrum for each selected spectral resolution.

| 256 fft length/spectral res. ($\Delta v = 0.08 \text{ m s}^{-1}$) | 512 fft length/spectral res. ($\Delta v = 0.04 \text{ m s}^{-1}$) | 1024 fft length/spectral res. ($\Delta v = 0.02 \text{ m s}^{-1}$) |
|---|---|--|
| 0.0512s | 0.1s | 0.2s |

Table 4. Number of averaged spectra to obtain each integration time for different n_{fft} cases.

| Integration time $\Delta T[s]$ | N_{spectra}^{256} | N_{spectra}^{512} | $N_{\text{spectra}}^{1024}$ |
|-----------------------------------|----------------------------|----------------------------|-----------------------------|
| 0.4 s | 8 | 4 | 2 |
| 2 s | 40 | 20 | 10 |
| 10 s | 200 | 100 | 50 |

Table 5. Bias and standard deviation of the difference of moments derived from corresponding spectra having different spectral resolutions.

| Non Drizzle | BIAS | | STD | | Drizzle | BIAS | | STD | |
|-------------|-----------|------------|-----------|------------|---------|-----------|------------|-----------|------------|
| | 256 – 512 | 512 – 1024 | 256 – 512 | 512 – 1024 | | 256 – 512 | 512 – 1024 | 256 – 512 | 512 – 1024 |
| Z_e | 0.28 | 0.32 | 0.89 | 1.16 | Z_e | 0.02 | 0.06 | 0.42 | 0.46 |
| V_d | 0.001 | -0.006 | 0.08 | 0.12 | V_d | -0.0011 | -0.0009 | 0.05 | 0.04 |
| S_w | 0.013 | 0.011 | 0.04 | 0.03 | S_w | 0.007 | 0.003 | 0.02 | 0.02 |
| S_k | -0.004 | -0.006 | 0.31 | 0.39 | S_k | -0.017 | 0.005 | 0.16 | 0.18 |



Table 6. Mean of distributions: 20 November 2014

| Mean of distributions: 20 November 2014 | | | | |
|---|---------------------------------|-----------|-----------|------------|
| Moments | Integration time ΔT [s] | nfft= 256 | nfft= 512 | nfft= 1024 |
| Reflectivity | 0.4 s | −43.0 | −43.3 | −43.1 |
| | 2.0 s | −44.5 | −45.0 | −45.0 |
| | 10 s | −46.0 | −46.0 | −46.1 |
| Mean Doppler Velocity | 0.4 s | 0.17 | 0.17 | 0.16 |
| | 2.0 s | 0.16 | 0.16 | 0.14 |
| | 10 s | 0.17 | 0.17 | 0.21 |
| Spectral width | 0.4 s | 0.13 | 0.11 | 0.11 |
| | 2.0 s | 0.15 | 0.16 | 0.13 |
| | 10 s | 0.17 | 0.16 | 0.15 |
| Skewness | 0.4 s | −0.04 | −0.01 | −0.005 |
| | 2.0 s | −0.04 | 0.01 | −0.1 |
| | 10 s | −0.08 | −0.07 | −0.06 |

Table 7. Mean of distributions: 24 June 2015

| Mean of distributions: 24 June 2015 | | | | |
|-------------------------------------|---------------------------------|-----------|-----------|------------|
| Moments | Integration time ΔT [s] | nfft= 256 | nfft= 512 | nfft= 1024 |
| Reflectivity | 0.4 s | −31.7 | −31.8 | −31.9 |
| | 2.0 s | −31.6 | −31.6 | −31.7 |
| | 10 s | −31.5 | −31.5 | −31.5 |
| Mean Doppler Velocity | 0.4 s | 0.25 | 0.26 | 0.26 |
| | 2.0 s | 0.26 | 0.26 | 0.26 |
| | 10 s | 0.26 | 0.26 | 0.26 |
| Spectral width | 0.4 s | 0.19 | 0.18 | 0.18 |
| | 2.0 s | 0.21 | 0.20 | 0.20 |
| | 10 s | 0.22 | 0.21 | 0.21 |
| Skewness | 0.4 s | 0.24 | 0.26 | 0.25 |
| | 2.0 s | 0.25 | 0.24 | 0.27 |
| | 10 s | 0.21 | 0.23 | 0.23 |



- Acknowledgements.* This research has received funding through Initial Training for Atmospheric Remote Sensing (ITARS; www.itars.net), European Union Seventh Framework Programme (FP7/2007–13): People, and ITN Marie Curie Actions Programme (2012–16) under Grant Agreement 289923 as well as from ACTRIS-2 (www.actris.eu) in the European Union’s Horizon 2020 research and innovation programme under grant agreement No 654109. Additionally, the cloud radar data management and interpretation has been funded by the research initiative
- 5 High Definition Clouds and Precipitation for advancing Climate Prediction HD(CP)2 I under grants FKZ01LK1209A and FKZ01LK1209B (PI Anne Hirsikko) funded by the German Ministry for Education and Research (BMBF). Further, the Transregional Collaborative Research Center TR32 Patterns in Soil–Vegetation–Atmosphere Systems, funded by the German Science Foundation (DFG), has contributed significantly to the maintenance of the cloud radar. The authors would like to thank all scientists taking part in the regular "cloud Doppler radar spectra skype meetings" for their interest and contribution regarding this work and, in addition, especially Susanne Crewell, Gabriele
- 10 Corbetta, Emiliano Orlandi, Paloma Borque and Andrés Pérez.